ACS APPLIED MATERIALS & INTERFACES

www.acsami.org

Research Article

Role of Surface Tension on Heat Feedback and Power from Energetic Composites

Yujie Wang, Feiyu Xu, George Issac Paul, Emmanuel Vidales Pasos, Keren Shi, Brandon Wagner, Lorenzo Mangolini, and Michael R. Zachariah*

Cite This: *ACS Appl. Mater. Interfaces* 2024, 16, 42100−42108

Read Online

ACCESS | Metrics & More | Article Recommendations | Supporting Information

ABSTRACT: Heat feedback to the unburned reaction interface is an important controlling factor of the velocity of the reaction front and power delivery. In this paper, we investigate the effect of agglomerate surface tension and its relationship to surface residence time and heat feedback on the combustion characteristics by Si addition to an Al/$KClO_4$ composite. Macroscopic imaging demonstrates a significant increase in burn rate with the addition of Si despite the fact that Si/$KClO_4$ has a slightly lower energy density than Al/$KClO_4$. Microscopic imaging coupled with three-color pyrometry reveals that molten liquid forms and evolves into spherical droplets on the burning surface, which are subsequently ejected from the surface. We find that the addition of Si results in a small increase in droplet size and a negligible impact on droplet temperature. However, the droplet formation rate on the surface is slower, leading to a significantly longer surface residence time. This leads to enhanced conductive heat feedback to the unburnt materials, thereby increasing the burn rate and energy release rate. We attribute the decreased droplet growth rate to the lowered surface tension of the liquid mixture with Si addition. This study highlights the crucial role of agglomerate physical property (e.g., surface tension) in influencing the combustion behavior of energetic composites.

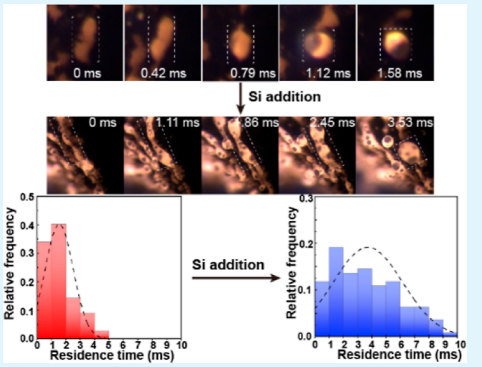

KEYWORDS: *agglomerate, surface tension, interface, combustion, energy release rate, heat feedback*

1. INTRODUCTION

The development of solid propellants using metals as high-energy fuel has gained growing interest in the quest for materials capable of achieving higher energy release rates.[1] Metalized energetics has emerged as a promising frontier due to their higher theoretically chemical energy density compared to the traditional CHNO energetics.[2−6] Despite the higher energy density, the relatively long diffusion length between fuel and oxidizer of traditional micrometer-scale metal energetics results in slow reaction kinetics. Modern formulations that incorporate nanoscale fuels and oxidizers aim to enhance reactivity by increasing the specific surface area and reducing the transport distances.[2,5,7−9] Aluminum (Al) nanoparticles have been widely used for this purpose due to their high gravimetric and volumetric energy density (31.1 $kJ{\cdot}g^{-1}$ and 83.8 $kJ{\cdot}cm^{-3}$, respectively), as well as ready availability.[10−15] However, agglomeration becomes prevalent with the replacement of micron scale Al with nanoscale Al.[16,17] This is because of the tendency of Al nanoparticles to aggregate, sinter, and coalesce due to either solid state diffusion or viscous flow.[1,18] The agglomeration mitigates the advantages of utilizing Al nanoparticles and decreases the energy release rate.[10,19,20]

Previous studies have explored various methods to improve the combustion performance of Al nanoparticles, such as surface coating,[21−23] utilizing an additive,[1] employing an unzipping polymer,[24] and assembling Al nanoparticles into mesoparticles.[19,25,26] While these studies primarily focus on reducing agglomeration, other factors significantly influence combustion performance, one of which is the heat feedback.[1,27−32] Sufficient heat feedback to the unreacted material is essential for the steady propagation of an energetic system,[31−33] and a higher amount of heat feedback has been proven to enhance the burn rate and energy release rate.[27,28,34] Despite these findings, an investigation focusing on the effect of agglomerate physical properties on the heat feedback and burn rate is still lacking and is the focus of this paper.

In this paper, we investigate the effect of agglomerate surface tension and its relationship to heat feedback on the combustion characteristics of 3D printed 90% loading Al/$KClO_4$ composites with Si addition (0, 10, and 25 wt %). Si is utilized, as Si/$KClO_4$ has a similar energy density to Al/$KClO_4$ (8.7 vs 9.5 kJ/g). In situ imaging techniques have been demonstrated to be particularly useful to study the combustion

Received: April 9, 2024
Revised: June 5, 2024
Accepted: July 5, 2024
Published: July 31, 2024

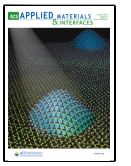

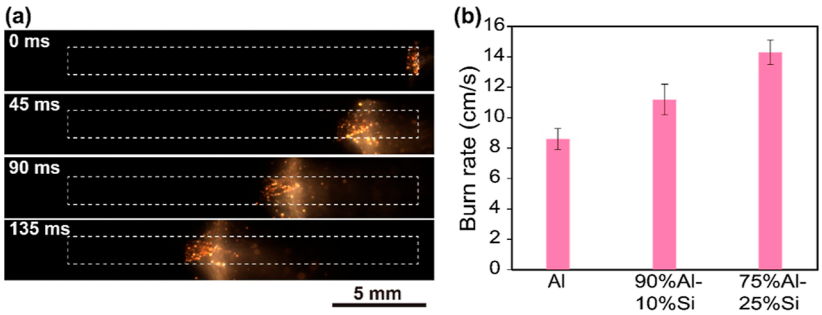

Figure 1. Time-resolved snapshots from high-speed macroscopic video of the composite of Al/$KClO_4$ (a). Dashed lines represent the printed composites before ignition. Measured burn rates of different composites (b). Images for the cases with Si addition appear qualitatively similar and can be found in Figure S4 in the Supporting Information.

behavior of aluminized energetic composites.[35−38] Here we employ high-speed microscopic imaging to study the reaction front and postflame with high temporal (μs) and spatial (μm) resolution.[16,24,39] This enables us to track the agglomerate size and surface residence time to provide information about the evolution process of agglomerates. Three-color imaging pyrometry is used to measure the temperature of the agglomerates. Burn rates of these composites are measured, and relative energy release rates are calculated. The different forces affecting a representative agglomerate on the burning surface are estimated and compared to determine the agglomerate detachment mechanism. Scanning electron microscopy (SEM) coupled with energy-dispersive spectrometry (EDS) and X-ray diffraction (XRD) are utilized to analyze the postcombustion product and provide insight into the combustion process. In this paper, we will explain why adding a fuel with a slightly lower energy density (Si) to Al can result in an energy release rate increase in power by 2X.

2. MATERIALS AND METHODS

2.1. Materials. Aluminum nanoparticles (Al NPs, ~ 70 nm) were purchased from US Research Nanomaterials. Potassium perchlorate ($KClO_4$, 99%) was obtained from Alfa Aesar. Polyvinylidene Fluoride (PVDF, average molecular weight: ~ 534,000) obtained from Sigma-Aldrich and METHOCEL F4M Hydroxypropyl Methylcellulose (HPMC) purchased from Dow Chemical Company were used as the binder for printing. *N*,*N*-dimethylformamide (DMF, 99.8%) was obtained from Fisher Scientific and used as a solvent to dissolve PVDF, HPMC, and $KClO_4$.

2.2. Synthesis of Silicon Nanoparticles. Silicon nanoparticles were synthesized via a nonthermal plasma method.[15,40] Briefly, the reactor is composed of a quartz tube (8 × 1 in.) and two copper ring electrodes. The first electrode was connected to an rf power supply (13.56 MHz) and matching network, and the second electrode was grounded. A butterfly valve was utilized to maintain a constant pressure of 267 Pa, and a baratron (MKS Baratron Capacitance Manometer) was used to monitor the pressure within the reactor. 1.36% SiH_4 and argon mixture was flown as the precursor gas while the rf input power was set at 80 W at to produce Si nanoparticles. The particles were collected downstream of the plasma volume by filtering.

2.3. Preparation of Ink and Direct Ink Writing of 90 wt % Loading Al−Si/$KClO_4$ Composites. Three stoichiometric 90 wt % loading composites were prepared with the fuel being Al and Si, and the oxidizer always being $KClO_4$. We refer to the samples in terms of the mass percentage of Al and Si in the fuel. For example, a 90% Al−10% Si sample means that 90% of the fuel is Al, 10% of is Si, and the corresponding amount of $KClO_4$ is used as the oxidizer to make the overall stoichiometric assuming complete conversion to Al_2O_3 and SiO_2. The details on preparing ink and printing the composites can be found in our previous study.[41] Briefly, 4 wt % of PVDF, 6 wt % of HPMC, and $KClO_4$ were dissolved into DMF. Every ink had a constant 25 mg/mL polymer binder in DMF. Then the fuel nanoparticles were added to the solution, which was ultrasonicated for 30 min and magnetically stirred overnight before printing. For printing with a Hyrel printer (SYSTEM 30 M), the ink was extruded through an 18-gauge needle on a preheated (~75 °C) substrate. The substrate was heated at ~75 °C for another 30 min when the printing was finished to ensure complete removal of DMF. The obtained films were cut into ~2 cm long sticks for the combustion investigation. Three composites, Al/$KClO_4$, 90% Al−10% Si/$KClO_4$, and 75% Al−25% Si/$KClO_4$, were prepared by 3D printing. For simplicity, these three composites are referred to as Al, 90% Al−10% Si, and 75% Al−25% Si, respectively. Details of the weight percentage of each component of all the composites are displayed in Table S1. SEM images of the cross sections for the three composites are shown in Figure S3.

2.4. Microscopic and Macroscopic Imaging. The details of the imaging process can be found in our previous publications.[16,42] Generally, the combustion process of the composites was studied with two imaging systems, one of which was the microscopic imaging system with a high-speed camera (Vision Research Phantom VEO710L) coupled with an Infinity Photo-Optical Model K2 DistaMax. The other imaging system was a macroscopic imaging system with high-speed camera (Vision Research Phantom Miro M110). For one measurement, a stick was positioned on a stage inside an argon-filled (1 atm) cubic chamber (edge length: 10 cm), which was placed between the two imaging systems. The stick was ignited with a Joule-heated nichrome wire, and the combustion process was recorded with both imaging systems. For determining the average burn rate along with standard error, a minimum of three tests were conducted on each composite.

For the droplet size measurement and residence time tracking from the microscopic imaging video, a minimum of 100 droplets were measured for each composite.

2.5. Electron Microscopy and X-ray Diffraction Crystallography. XRD [Empyrean PANalytical Series 2; Cu-Kα source (λ = 1.541 Å)] was used to characterize the as-synthesized Si nanoparticles (Figure S1) and composition of the postcombustion product of Al/$KClO_4$ and 75% Al−25% Si/$KClO_4$. The size and morphology of Si nanoparticles were characterized by TEM (120 kV accelerating voltage; Thermo Fisher Scientific Talos L120C; Figure S2). SEM (Thermo Fisher Scientific NNS450) coupled with energy dispersive X-ray spectroscopy (EDS) was used to analyze the morphology and composition of the postcombustion product. Postcombustion product was collected inside a glass tube (ID: 1 in.) filled with argon. For 75% Al−25% Si/$KClO_4$, the obtained product was washed with water briefly to dissolve KCl nanoparticles, which is formed during combustion, to simplify the XRD spectrum.[16] To minimize oxidation of the particles in water, the washing process involved adding water to the postcombustion product and vigorously vortexing it for approximately 20 s. Subsequently, the suspension was promptly centrifuged, the precipitate was collected, and it was then dried under vacuum in a desiccator before conducting SEM and XRD analysis.

https://doi.org/10.1021/acsami.4c05801
ACS Appl. Mater. Interfaces 2024, 16, 42100−42108

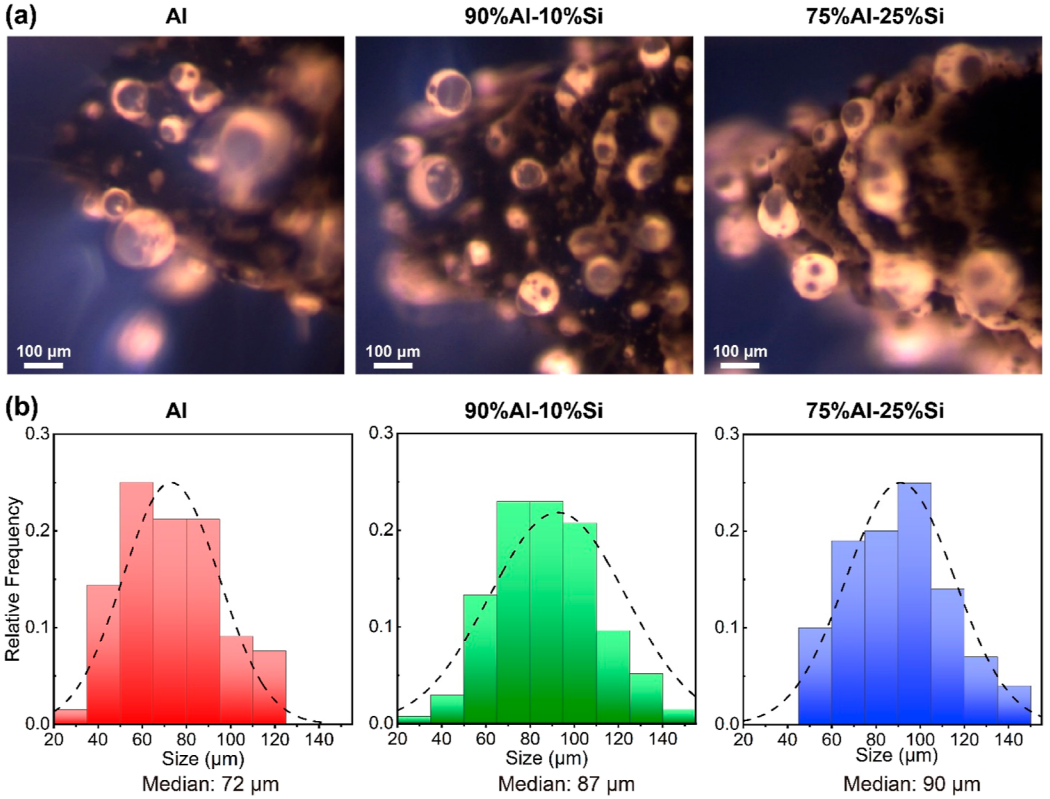

Figure 2. Images from high-speed microscopic video (a) and droplet size distribution (b) for the composites of Al, 90% Al−10% Si, and 75% Al−25% Si.

2.6. Three-Color Imaging Pyrometry. Details about three-color imaging pyrometry can be found in previous publications from our group.[31,39,43] In general, temperature measurements of the sample were conducted by analyzing the ratios of channel intensities in three colors (red, green, and blue) captured through the Bayer filter. This analysis was performed by using a custom MATLAB routine, assuming that the sample exhibited graybody emission behavior. Calibration factors were determined with a blackbody source (Mikron M390). The estimated temperature uncertainty is typically within the range of 200−300 K.[27,31]

3. RESULTS AND DISCUSSION

Combustion behaviors of the Al, 90% Al−10% Si, and 75% Al−25% Si composites were characterized with high-speed macroscopic and microscopic cameras in argon. (For simplicity, $KClO_4$ is excluded in the name of these composites). A series of time-resolved snapshots of these composites from macroscopic video are shown in Figures 1 and S4. All three composites show stable and linear propagation, and the burn rate increases as the Si content increases, as displayed in Figures 1a and S4. Figure 1b shows that the macroscopic burn rate is 8.6 11.2, and 14.3 cm/s for Al, 90% Al−10% Si, and 75% Al−25% Si, respectively. It is noteworthy that while previous studies has demonstrated that the increase in porosity results in a higher burn rate,[44] the porosity of the composite was largely unaffected by Si addition in our composites (all composites have porosity near 50%). Therefore, the observed increase in burn rate cannot be explained by the porosity increase.

Microscopic videos provide important insight into the combustion characteristics of a composite by enabling the direct observation of combustion events on the burning surface. Figure 2a shows the snapshots from high-speed microscopic videos of the composites with different Si contents. Cone-shaped flame front is observed for all three composites and is attributed to a higher porosity on the edge of the composites that arises from a higher solvent evaporation rate during printing.[16] For the composite of bare Al, molten droplets with dark caps form on the burning surface. The main (bright) body of these droplets is almost pure Al while the dark cap consists of Al_2O_3.[16,45] These mobile droplets coalesce and/or absorb newly formed liquid nearby, growing into larger droplets before departing from the burning surface.[46] The incorporation of 10 and 25% Si has a minimal influence on the morphology of the droplets, as shown in Figure 2a. Droplet sizes of the three composites are measured, and the distributions are displayed in Figure 2b, which illustrates that the addition of Si slightly increases the droplet size.

Three-color (RGB) pyrometry is utilized to measure the temperature of the flame front, and the representative temperature maps of the composites with different Si contents are displayed in Figure 3a. For the composite with bare Al, main body of the droplets have an average temperature of ∼2350 K, which is significantly higher than the melting point of Al at 930 K. It is noteworthy that this measured temperature is approximately equal to the melting point of Al_2O_3 at 2345 K.[37] At this temperature Al_2O_3 melts and retracts, forming a distinct lobe due to surface tension.[16,47] With the introduction of Si to the composite, the average temperature of the main body of the droplets is ∼2450 K for 90% Al−10% Si and ∼2500 K for 75% Al−25% Si, respectively. The droplet temperature difference between bare Al and 75% Al−25% Si is within the uncertainty of the measurement (200−300 K),[27,31] therefore we conclude that the addition of Si has minimal effect on the droplet temperature. For droplets of all three

https://doi.org/10.1021/acsami.4c05801
ACS Appl. Mater. Interfaces 2024, 16, 42100−42108

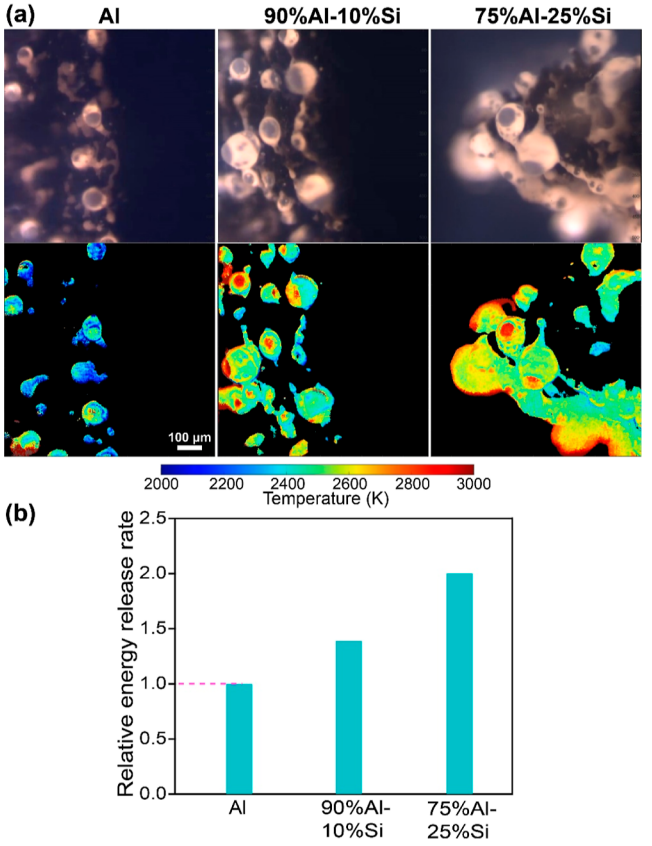

Figure 3. Temperature maps from three-color pyrometry (a) and estimated relative energy release rates (b) for the composites of Al, 90% Al−10% Si, and 75% Al−25% Si. High error points and low-intensity points were excluded from the temperature measurement. Details about relative energy release rate estimation can be found in the Supporting Information (Section S2).

composites, the temperature of Al_2O_3 cap is higher than the main body, consistent with the observations from previous studies.[16,37]

Combustion performance of different composites can be evaluated by comparing their energy release rate. Figure 3b shows the relative energy release rate of the three composites. It is evident that the energy release rate of the composite increases with the addition of Si. As the Si content increases from 10 to 25%, the relative energy release rate rises from 1.4- to-2.0 times that of bare Al. Given that the gravimetric energy density of $Si/KClO_4$ is lower than $Al/KClO_4$ (8.7 vs 9.5 kJ/g), the observed increase in energy release rate cannot be explained by theoretical energy density difference. In addition, previous studies have demonstrated that the smaller agglomeration size favors a higher burn rate.[1,24,27,34] As shown in Figure 2b, the droplet size of the composite slightly increases with Si addition. A primary question now arises: Why does the introduction of Si significantly increase the energy release rate?

Microscopic imaging videos demonstrate that the initial agglomerates require some time to evolve into droplets, which then reside on the burning surface for a period of time before departure rather than being ejected immediately after formation. Figure 4a presents a series of snapshots depicting a representative process from agglomerate emergence, droplet formation, growth, and departure from the burning surface of the bare Al composite. Agglomerate surface residence time is estimated by tracking the time span from the emergence of the agglomerate that evolves into a droplet to the departure of that droplet, and the obtained distributions for different composites are shown in Figure 4b, which shows that the addition of Si clearly increases the agglomerate surface residence time. The vast majority of the agglomerate residence time for bare Al composite is below 3 ms. With 10% Si introduction, the overall agglomerate residence time increases, and approximately 35% of agglomerates have residence time exceeding 3 ms. As the Si content increases from 10 to 25%, the overall agglomerate residence time continues to rise, with more than 60% of agglomerates having a residence time exceeding 3 ms.

Steady propagation requires the transfer of sufficient heat from the flame back to the unreacted material.[31−34,48] Conduction, convection, and radiation are the three primary methods for heat transfer. Previous studies have demonstrated that radiative heat feedback is negligible for a propellant

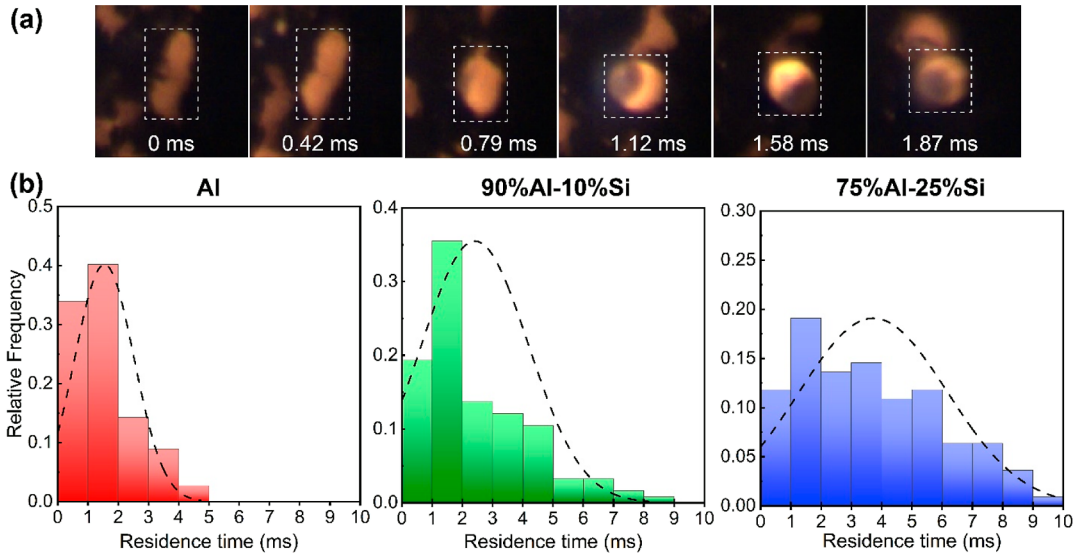

Figure 4. Time-resolved snapshots of the evolution of a representative droplet from emergence to departure from the burning surface for the composite of bare Al (a). Measured agglomerate surface residence time distribution of Al, 90% Al−10% Si, and 75% Al−25% Si (b).

https://doi.org/10.1021/acsami.4c05801
ACS Appl. Mater. Interfaces 2024, 16, 42100−42108

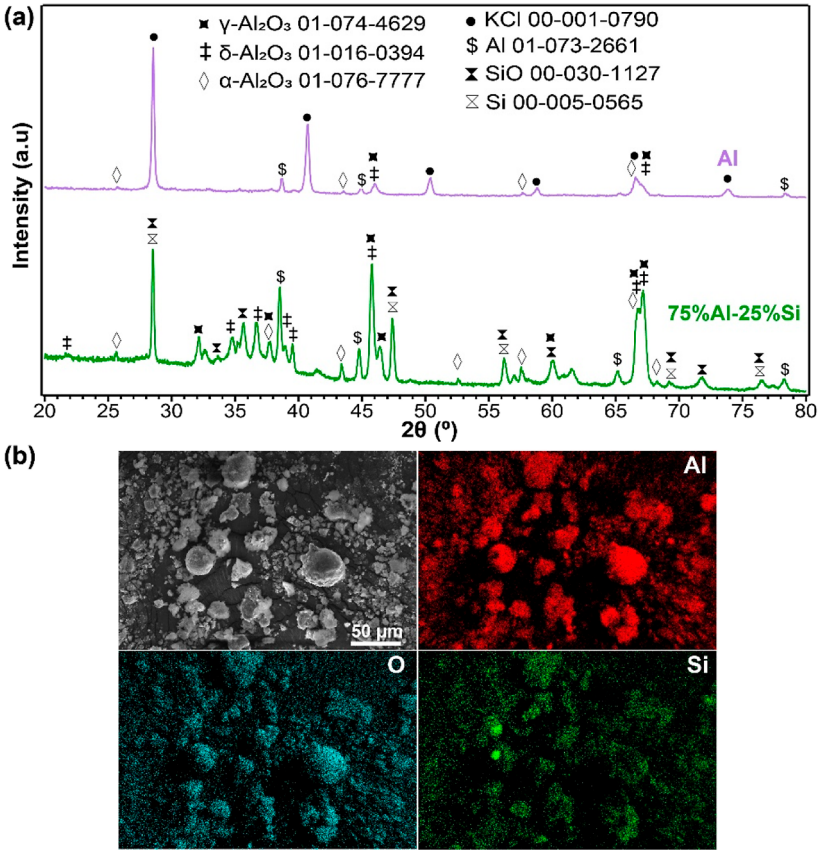

Figure 5. XRD spectra of postcombustion products from the composites of bare Al and 75% Al−25% Si (a). SEM image and corresponding EDS images of postcombustion products of the 75% Al−25% Si composite (b). Note: product of the 75% Al−25% Si composite was water-washed briefly to remove KCl for obtaining a cleaner XRD spectrum and allowing large agglomerates to remain on the carbon tap for SEM.

propagating at atmospheric pressure.[32,33,48,49] In the current study, combustion tests of the composites were conducted inside a vented chamber to maintain approximate atmospheric pressure; therefore, we disregard the effect of radiative heat feedback. Convective heat transfer can be further divided into convection of gas and convection from the movement of condensed phase material.[33,50−52] Egan and Zachariah investigated gas convection in an Al/CuO system propagating inside a narrow channel and concluded that convective heat transfer was insufficient to sustain combustion.[33] Calculation shows that Al−Si/$KClO_4$ has less gas generation compared to Al/CuO, assuming that the oxygen produced from the oxidizers is completely consumed by Al. While the composite of Al−Si/$KClO_4$ has 10% polymer binder (4% PVDF and 6% HPMC), prior work has demonstrated this polymer mixture has little gas release.[24] It is noteworthy that the combustion test of the composite in the current study was conducted inside a chamber with a cross-section area approximately 4 orders of magnitude higher than that of a composite stick. This indicates that convective heat transfer effect is much lower than the significantly confined Al/CuO system studied by Egan and Zachariah,[33] therefore the effect of convective heat transfer of gas is insignificant. As for the effect caused by the movement of condensed phase material, no movement of the burning droplet back to the unburnt composite is observed from the microscopic imaging. This can be attributed to the lack of confinement effect from the test chamber, given that its cross-sectional area is drastically larger than that of the composite stick. Thus, it can be concluded that the convective heat transfer effect is insignificant for the propagation of Al−Si/$KClO_4$ composites.

From the discussion so far, we can conclude that the radiation heat feedback is negligible and convection is not the dominant mode of energy transport for the propagation of Al−Si/$KClO_4$ composites. The remaining mechanism is conduction heat transfer. The significance of conductive heat transfer has been suggested previously. Brewster and Hardt concluded that the residence of metal agglomerates on or near the surface of a propellant tended to increase the burn rate of the propellant by transferring heat to the propellant.[34] Our prior work of Wang et al. demonstrated the addition of carbon fiber increased the burn rate of Al/CuO by enhancing conductive heat transfer from hot burned/burning particles to the unburnt materials.[27] In the current study, we have shown that agglomerate residence time increases with Si addition (Figure 4b), suggesting an increase in conductive heat feedback to the unburnt material, which enhances the burn rate. A new question now arises: Why does the addition of Si increase the agglomerate residence time? To answer this question, we will primarily compare the composites of bare Al and 75% Al−25% Si.

XRD and SEM/EDS were utilized to analyze the postcombustion products. Figure 5a displays the XRD results of postcombustion product from the composites of bare Al and 75% Al−25% Si. In the composite of bare Al, KCl resulting from the decomposition of $KClO_4$, unreacted Al, γ-phase Al_2O_3, δ-phase Al_2O_3, and α-phase Al_2O_3 are present. In the composite of 75% Al−25% Si, in addition to the components

https://doi.org/10.1021/acsami.4c05801
ACS Appl. Mater. Interfaces 2024, 16, 42100−42108

observed for the bare Al composite, SiO, and unreacted Si are identified. These results suggest the incomplete combustion of Al and Si. As discussed in the previous section, for the composite of bare Al, the main body of the droplets during combustion is almost pure Al while the dark cap is Al_2O_3.[16,45] SEM/EDS images in Figure 5b show that for the 75% Al−25% Si composite, aluminum, oxygen, and silicon are homogeneously distributed on the surface of the particles except for a few small spots. Al and Si are miscible at any atomic ratio when the temperature is above the melting point of Si at 1414 °C,[53] which is significantly lower than the measured temperature of main body of the droplets (>2100 °C). This suggests that for the composites with Si addition, the main body of the droplets forms a homogeneous mixture of Al and Si, consistent with the EDS analysis that Al and Si are homogeneously distributed on the postcombustion particles. For simplicity in the following discussion, we assume Al and Si are in the main body, while SiO and Al_2O_3 are in the cap for the burning droplets of composites with Si addition.

Now, let us consider the forces that a droplet feels in order to detach from the burning surface. On the burning surface the droplet will experience aerodynamic forces (drag or blowing force) due to gas flow effusing from surface, adhesive forces, and gravity, as shown in Figure 6a.[29,54,55] Gravity plays an

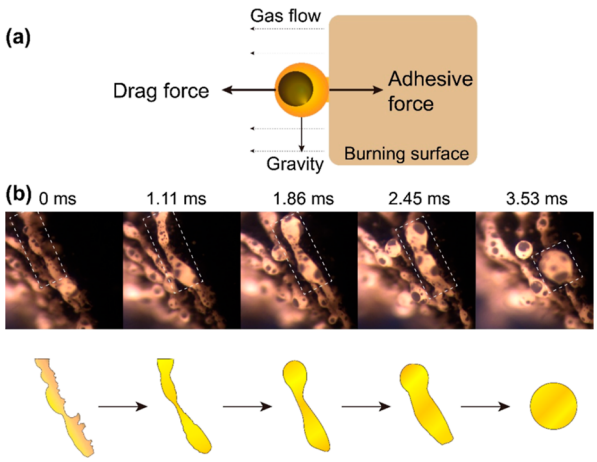

Figure 6. Schematic of the forces experienced by a droplet on a burning surface (a). Representative dewetting process (top) and the corresponding illustration (bottom) for the composite of 75% Al−25% Si (b).

insignificant role in droplet detachment, as no consistent downward movement is observed for the departed droplets. We begin by assuming that the surface generates gas (blowing force), which will want to lift the particle from the surface by a drag force. To estimate the drag force, we need to know the blowing velocity at the surface of the attachment. To do this, however, we measure the velocity of the departed particle, assuming it has reached its terminal velocity, and assuming it is equivalent to the blowing velocity. We can then calculate the lifting force from Stokes Law (i.e., the drag force; F_{drag}) shown in eq 1.[56] Where C_D is drag coefficient, ρ_g is the gas density, d is the diameter of the particle, and v is the relative velocity of the gas flow. Counteracting the drag (or detachment) force is the adhesive force (F_{adh}) characterized by eq 2.[56] The adhesive force arises from the combination of van der Waals, electrostatic, and surface tension forces, which are represented by the first, second, and third terms on the right side of eq 2, respectively.

$$F_{drag} = C_D \frac{\pi}{8} \rho_g d^2 v^2 \tag{1}$$

$$F_{adh} = \frac{Ad}{12x^2} + \frac{K_\varepsilon q^2}{x_q^2} + 2\pi\gamma d \tag{2}$$

where A is the Hamaker constant, x is the distance between the particle and the plane surface, K_ε is the constant of proportionality, x_q is the separation distance of opposite charges, and γ is the surface tension of the liquid between the particle and the plane surface. For order-of-magnitude estimates we will consider a representative droplet (d = 100 μm, temperature = 2500 K). Velocity tracking of the droplet leads to an average velocity of ∼2 m/s, C_D is estimated to be 1,[56] and the gas density (ρ_g) is assumed to be the density of argon (1.6 kg/m^3). A drag force (F_{drag}) from eq 1 yields a value of 3×10^{-8} N.

In estimating the adhesive force (F_{adh}), we can safely neglect the electrostatic force as the droplet primarily consists of conductive Al, so it is unlikely that charge on the droplet accumulates due to the contact with the burning surface. Given the wetting behavior of these droplets as evidenced by the clear liquid Al bridge (Figure S5), van der Waals forces are likely to be much smaller than surface tension forces. In the calculation of surface tension, the adhesive force, γ_{Al} is estimated to be 0.6 N/m at 2500 K,[57] resulting in a surface tension adhesive force of $\sim 4 \times 10^{-4}$ N. This is orders of magnitude higher than the blowing force (drag force; $\sim 3 \times 10^{-8}$ N), suggesting that gas generation at the surface is too small to detach the droplet from the burning surface. Previous studies have shown that for the detachment of particles from surfaces, the lifting force usually contributes less than tangential forces acting parallel to the surface, which results in rolling or sliding of particles.[58,59] In the current study, droplet rolling on the burning surface is commonly observed, and we believe it to be the primary cause of droplet detachment. The observed droplet rolling is attributed to the flow dynamics inside the droplet at a high temperature (2500 K), which remain consistent for droplets with different sizes due to the invariant temperature among these droplets.[60] Basu et al. demonstrated that the critical shear rate for the detachment of a partially wetting droplet decreases as the droplet size increases.[61] Thus, a droplet needs to grow to a sufficient size to reach the critical shear rate for detachment. This explains the relatively large droplet size (∼100 μm) observed for the detachment.

The preceding discussion primarily focused on the droplet detachment mechanism for the composite of bare Al but did not address why the addition of Si results in a higher surface residence time. As discussed above, a critical size must be achieved before a droplet can detach. To achieve this critical size, neighboring droplets must fuse. The fusion occurs through viscous flow, and the characteristic fusion time (τ_F) can be calculated using Frenkel's law[17,62] in eq 3.

$$\tau_F = \frac{\pi\eta d}{\gamma} \tag{3}$$

where η is the viscosity, γ is the surface tension. For Al at 2500 K, the surface tension is estimated to be 0.6 N/m and the viscosity is estimated to be 0.48 mPa·s.[57,63] For two droplets with a diameter of 100 μm, the computed characteristic fusion

https://doi.org/10.1021/acsami.4c05801
ACS Appl. Mater. Interfaces 2024, 16, 42100−42108

time is ~2.5 × 10^{-4} ms. This is a few orders of magnitude smaller than the overall measured droplet surface residence time and can therefore be neglected.

Another contributing factor to the surface residence time is the time required for the liquid to evolve into a droplet. Microimaging videos show the formation of burning liquid "pool" before its evolution into a spherical droplet (Figures 4a and 6b). The process for the liquid "pool" evolving into a droplet can be regarded as dewetting of the burning surface by the liquid fuel.[64] Bertrand et al. demonstrated that growth rate of the droplet for dewetting is related to the surface tension of the liquid, and a higher surface tension results in a higher droplet growth rate.[64] With the introduction of Si, the surface tension of the mixture decreases as $\gamma_{Si} < \gamma_{Al}$ at 2500 K (0.25 N/m vs 0.6 N/m).[57] Consequently, the droplet growth rate decreases and more time is required for the liquid to evolve into a droplet. Figure 6b displays a representative dewetting process for the 75% Al−25% Si composite with a measured dewetting time of ~3.5 ms, which is significantly longer than the total surface residence time for a representative droplet of the bare Al composite (Figure 4a). This explains why the introduction of Si increases the agglomerate surface residence time.

4. CONCLUSIONS

This paper investigates the effect of agglomerate surface tension on heat feedback and burn rate of energetic composites by studying the combustion behavior of Al/$KClO_4$ composites with Si as an additive. The introduction of Si significantly increases the burn rate and the energy release rate. Microscopic imaging shows that droplets resulting from the evolution of molten liquid form on the burning surface, and the addition of Si has minimal impact on the droplet temperature while slightly increasing the droplet size. However, the lower surface tension of Si compared to Al decreases the overall liquid surface tension, leading to a lower droplet growth rate and a longer time required for the liquid to transform into droplets. This results in a prolonged agglomerate surface residence time and, consequently, enhanced conductive heat feedback to the unburnt materials, ultimately increasing the burn rate and energy release rate. This study illustrates the crucial role of agglomerate surface tension in impacting the combustion behavior of energetic composites.

■ ASSOCIATED CONTENT

Supporting Information

The Supporting Information is available free of charge at https://pubs.acs.org/doi/10.1021/acsami.4c05801.

XRD spectrum of Si nanoparticles; TEM image of the as-synthesized Si nanoparticles; SEM images of cross-section for the printed composites; time resolved-snapshots from high-speed macroscopic video of the composites; droplet before and after detachment from the burning surface; andmass percentage of Al, Si, $KClO_4$, and polymer for different composites (PDF)

■ AUTHOR INFORMATION

Corresponding Author

Michael R. Zachariah − *University of California, Riverside, California 92521, United States;* orcid.org/0000-0002-4115-3324; Email: mrz@engr.ucr.edu

Authors

Yujie Wang − *University of California, Riverside, California 92521, United States*

Feiyu Xu − *University of California, Riverside, California 92521, United States*

George Issac Paul − *University of California, Riverside, California 92521, United States*

Emmanuel Vidales Pasos − *University of California, Riverside, California 92521, United States*

Keren Shi − *University of California, Riverside, California 92521, United States*

Brandon Wagner − *University of California, Riverside, California 92521, United States*

Lorenzo Mangolini − *University of California, Riverside, California 92521, United States;* orcid.org/0000-0002-0057-2450

Complete contact information is available at: https://pubs.acs.org/10.1021/acsami.4c05801

Author Contributions

Yujie Wang: Conceptualization, methodology, data curation, writing—original draft; and writing—review and editing. Feiyu Xu: Conceptualization, data curation, writing—review and editing. George Issac Paul: Methodology, data curation, writing—review and editing. Emmanuel Vidales Pasos: Data curation, writing—review and editing. Keren Shi: Data curation, writing—review and editing. Brandon Wagner: Data curation, writing—review and editing. Lorenzo Mangolini: Investigation, validation, writing—review and editing. Michael R. Zachariah: Supervision, investigation, validation, project administration, writing—review and editing. All authors have given approval to the final version of the manuscript.

Notes

The authors declare no competing financial interest.

■ REFERENCES

(1) Sippel, T. R.; Son, S. F.; Groven, L. J. Aluminum Agglomeration Reduction in a Composite Propellant Using Tailored Al/PTFE Particles. *Combust. Flame* **2014**, *161* (1), 311−321.

(2) Rehwoldt, M. C.; Wang, H.; Kline, D. J.; Wu, T.; Eckman, N.; Wang, P.; Agrawal, N. R.; Zachariah, M. R. Ignition and Combustion Analysis of Direct Write Fabricated Aluminum/Metal Oxide/PVDF Films. *Combust. Flame* **2020**, *211*, 260−269.

(3) Comet, M.; Martin, C.; Klaumünzer, M.; Schnell, F.; Spitzer, D. Energetic Nanocomposites for Detonation Initiation in High Explosives without Primary Explosives. *Appl. Phys. Lett.* **2015**, *107* (24), 243108.

(4) Yen, N. H.; Wang, L. Y. Reactive Metals in Explosives. *Propellants Explos. Pyrotech.* **2012**, *37* (2), 143−155.

(5) He, W.; Liu, P.-J.; He, G.-Q.; Gozin, M.; Yan, Q.-L. Highly Reactive Metastable Intermixed Composites (MICs): Preparation and Characterization. *Adv. Mater.* **2018**, *30* (41), 1706293.

(6) Jian, G.; Piekiel, N. W.; Zachariah, M. R. Time-Resolved Mass Spectrometry of Nano-Al and Nano-Al/CuO Thermite under Rapid Heating: A Mechanistic Study. *J. Phys. Chem. C* **2012**, *116* (51), 26881−26887.

(7) Sundaram, D.; Yang, V.; Yetter, R. A. Metal-Based Nanoenergetic Materials: Synthesis, Properties, and Applications. *Prog. Energy Combust. Sci.* **2017**, *61*, 293−365.

(8) Comet, M.; Martin, C.; Schnell, F.; Spitzer, D. Nanothermites: A Short Review. Factsheet for Experimenters, Present and Future Challenges. *Propellants Explos. Pyrotech.* **2019**, *44* (1), 18−36.

(9) Granier, J. J.; Pantoya, M. L. Laser Ignition of Nanocomposite Thermites. *Combust. Flame* **2004**, *138* (4), 373−383.

(10) Yetter, R. A. Progress towards Nanoengineered Energetic Materials. *Proc. Combust. Inst.* **2021**, *38* (1), 57−81.
(11) Sami, Y.; Richard, N.; Gauchard, D.; Estève, A.; Rossi, C. Selecting Machine Learning Models to Support the Design of Al/CuO Nanothermites. *J. Phys. Chem. A* **2022**, *126* (7), 1245−1254.
(12) Young, G.; Wang, H.; Zachariah, M. R. Application of Nano-Aluminum/Nitrocellulose Mesoparticles in Composite Solid Rocket Propellants. *Propellants Explos. Pyrotech.* **2015**, *40* (3), 413−418.
(13) DeLuca, L. T.; Galfetti, L.; Colombo, G.; Maggi, F.; Bandera, A.; Babuk, V. A.; Sinditskii, V. P. Microstructure Effects in Aluminized Solid Rocket Propellants. *J. Propuls. Power* **2010**, *26* (4), 724−732.
(14) Galfetti, L.; Luca, L. T. D.; Severini, F.; Meda, L.; Marra, G.; Marchetti, M.; Regi, M.; Bellucci, S. Nanoparticles for Solid Rocket Propulsion. *J. Phys.: Condens. Matter* **2006**, *18* (33), S1991−S2005.
(15) Xu, F.; Nava, G.; Biswas, P.; Dulalia, I.; Wang, H.; Alibay, Z.; Gale, M.; Kline, D. J.; Wagner, B.; Mangolini, L.; Zachariah, M. R. Energetic Characteristics of Hydrogenated Amorphous Silicon Nanoparticles. *Chem. Eng. J.* **2022**, *430*, 133140.
(16) Wang, Y.; Hagen, E.; Biswas, P.; Wang, H.; Zachariah, M. R. Imaging the Combustion Characteristics of Al, B, and Ti Composites. *Combust. Flame* **2023**, *252*, 112747.
(17) Chakraborty, P.; Zachariah, M. R. Do Nanoenergetic Particles Remain Nano-Sized during Combustion? *Combust. Flame* **2014**, *161* (5), 1408−1416.
(18) Zachariah, M. R.; Carrier, M. J. Molecular Dynamics Computation of Gas-Phase Nanoparticle Sintering: A Comparison with Phenomenological Models. *J. Aerosol Sci.* **1999**, *30* (9), 1139−1151.
(19) Wang, H.; Jian, G.; Egan, G. C.; Zachariah, M. R. Assembly and Reactive Properties of Al/CuO Based Nanothermite Microparticles. *Combust. Flame* **2014**, *161* (8), 2203−2208.
(20) Dreizin, E. L. Metal-Based Reactive Nanomaterials. *Prog. Energy Combust. Sci.* **2009**, *35* (2), 141−167.
(21) He, W.; Lyu, J.-Y.; Tang, D.-Y.; He, G.-Q.; Liu, P.-J.; Yan, Q.-L. Control the Combustion Behavior of Solid Propellants by Using Core-Shell Al-Based Composites. *Combust. Flame* **2020**, *221*, 441−452.
(22) Zhang, J.; Zhao, F.; Li, H.; Yuan, Z.; Zhang, M.; Yang, Y.; Pei, Q.; Wang, Y.; Chen, X.; Qin, Z. Improving Ignition and Combustion Performance of Al@Ni in CMDB Propellants: Effect of Nickel Coating. *Chem. Eng. J.* **2023**, *456*, 141010.
(23) Kim, D. W.; Kim, K. T.; Lee, D.-U.; Jung, S.-H.; Yang, D. Y.; Yu, J. Influence of Poly(Vinylidene Fluoride) Coating Layer on Exothermic Reactivity and Stability of Fine Aluminum Particles. *Appl. Surf. Sci.* **2021**, *551*, 149431.
(24) Wang, H.; Wang, Y.; Garg, M.; Moore, J. S.; Zachariah, M. R. Unzipping Polymers Significantly Enhance Energy Flux of Aluminized Composites. *Combust. Flame* **2022**, *244*, 112242.
(25) Wang, H.; Jacob, R. J.; DeLisio, J. B.; Zachariah, M. R. Assembly and Encapsulation of Aluminum NP's within AP/NC Matrix and Their Reactive Properties. *Combust. Flame* **2017**, *180*, 175−183.
(26) Chowdhury, M.; Ghildiyal, P.; Rojas, A.; Wang, Y.; Wang, H.; Zachariah, M. R. High-Yield Spray Drying Assembly and Reactive Properties of Nanoenergetic Mesoparticle Composites. *Adv. Powder Technol.* **2023**, *34* (7), 104075.
(27) Wang, H.; Kline, D. J.; Rehwoldt, M. C.; Zachariah, M. R. Carbon Fibers Enhance the Propagation of High Loading Nanothermites: In Situ Observation of Microscopic Combustion. *ACS Appl. Mater. Interfaces* **2021**, *13*, 30504−30511.
(28) Wang, H.; Hagen, E.; Shi, K.; Herrera, S.; Xu, F.; Zachariah, M. R. Carbon Fibers as Additives to Engineer Agglomeration and Propagation of Aluminized Propellants. *Chem. Eng. J.* **2023**, *460*, 141653.
(29) Ao, W.; Fan, Z.; Liu, L.; An, Y.; Ren, J.; Zhao, M.; Liu, P.; Li, L. K. B. Agglomeration and Combustion Characteristics of Solid Composite Propellants Containing Aluminum-Based Alloys. *Combust. Flame* **2020**, *220*, 288−297.
(30) Liu, L.; Sang, L.; Gou, D.; Wen, Z.; Zhang, G.; Liu, P.; He, G.; Ao, W. Controlling the Combustion and Agglomeration Characteristics of Solid Propellants via New Micro-Unit Composite Fuel Al@AP. *Combust. Flame* **2023**, *258*, 113107.
(31) Kline, D. J.; Alibay, Z.; Rehwoldt, M. C.; Idrogo-Lam, A.; Hamilton, S. G.; Biswas, P.; Xu, F.; Zachariah, M. R. Experimental Observation of the Heat Transfer Mechanisms That Drive Propagation in Additively Manufactured Energetic Materials. *Combust. Flame* **2020**, *215*, 417−424.
(32) Summerfield, M. *Solid Propellant Rocket Research*; Elsevier, 2013.
(33) Egan, G. C.; Zachariah, M. R. Commentary on the Heat Transfer Mechanisms Controlling Propagation in Nanothermites. *Combust. Flame* **2015**, *162* (7), 2959−2961.
(34) Brewster, M. Q.; Hardt, B. E. Influence of Metal Agglomeration and Heat Feedback on Composite Propellant Burning Rate. *J. Propuls. Power* **1991**, *7* (6), 1076−1078.
(35) Melcher, J. C.; Krier, H.; Burton, R. L. Burning Aluminum Particles Inside a Laboratory-Scale Solid Rocket Motor. *J. Propuls. Power* **2002**, *18* (3), 631−640.
(36) Karasev, V. V.; Onischuk, A. A.; Glotov, O. G.; Baklanov, A. M.; Maryasov, A. G.; Zarko, V. E.; Panfilov, V. N.; Levykin, A. I.; Sabelfeld, K. K. Formation of Charged Aggregates of Al2O3 Nanoparticles by Combustion of Aluminum Droplets in Air. *Combust. Flame* **2004**, *138* (1−2), 40−54.
(37) Chen, Y.; Guildenbecher, D. R.; Hoffmeister, K. N. G.; Cooper, M. A.; Stauffacher, H. L.; Oliver, M. S.; Washburn, E. B. Study of Aluminum Particle Combustion in Solid Propellant Plumes Using Digital In-Line Holography and Imaging Pyrometry. *Combust. Flame* **2017**, *182*, 225−237.
(38) Marsh, A. W.; Wang, G. T.; Heyborne, J. D.; Guildenbecher, D. R.; Mazumdar, Y. C. Time-Resolved Size, Velocity, and Temperature Statistics of Aluminum Combustion in Solid Rocket Propellants. *Proc. Combust. Inst.* **2021**, *38* (3), 4417−4424.
(39) Wang, H.; Kline, D. J.; Zachariah, M. R. In-Operando High-Speed Microscopy and Thermometry of Reaction Propagation and Sintering in a Nanocomposite. *Nat. Commun.* **2019**, *10* (1), 3032.
(40) Mangolini, L.; Thimsen, E.; Kortshagen, U. High-Yield Plasma Synthesis of Luminescent Silicon Nanocrystals. *Nano Lett.* **2005**, *5* (4), 655−659.
(41) Wang, H.; Shen, J.; Kline, D. J.; Eckman, N.; Agrawal, N. R.; Wu, T.; Wang, P.; Zachariah, M. R. Direct Writing of a 90 Wt% Particle Loading Nanothermite. *Adv. Mater.* **2019**, *31* (23), 1806575.
(42) Wang, H.; Julien, B.; Kline, D.; Alibay, Z.; Rehwoldt, M.; Rossi, C.; Zachariah, M. Probing the Reaction Zone of Nanolaminates at ∼ μs Time and ∼ μm Spatial Resolution. *J. Phys. Chem. C* **2020**, *124* (25), 13679−13687.
(43) Jacob, R. J.; Kline, D. J.; Zachariah, M. R. High Speed 2-Dimensional Temperature Measurements of Nanothermite Composites: Probing Thermal vs. Gas Generation Effects. *J. Appl. Phys.* **2018**, *123* (11), 115902.
(44) Wu, T.; Julien, B.; Wang, H.; Pelloquin, S.; Esteve, A.; Zachariah, M. R.; Rossi, C. Engineered Porosity-Induced Burn Rate Enhancement in Dense Al/CuO Nanothermites. *ACS Appl. Energy Mater.* **2022**, *5* (3), 3189−3198.
(45) Dreizin, E. L. Experimental Study of Stages in Aluminium Particle Combustion in Air. *Combust. Flame* **1996**, *105* (4), 541−556.
(46) Rashkovskii, S. A. Role of the Structure of Heterogeneous Condensed Mixtures in the Formation of Agglomerates. *Combust. Explos. Shock Waves* **2002**, *38* (4), 435−445.
(47) Harrison, J.; Brewster, M. Q. Analysis of Thermal Radiation from Burning Aluminium in Solid Propellants. *Combust. Theory Model.* **2009**, *13* (3), 389−411.
(48) Ishihara, A.; Brewster, M. Q.; Sheridan, T. A.; Krier, H. The Influence of Radiative Heat Feedback on Burning Rate in Aluminized Propellants. *Combust. Flame* **1991**, *84* (1−2), 141−153.
(49) Horton, M. D.; Youngber, L. Z. Effect of Radiant Energy on the Burning Rate of a Composite Solid Propellant. *AIAA J.* **1970**, *8* (10), 1738−1741.

https://doi.org/10.1021/acsami.4c05801
ACS Appl. Mater. Interfaces 2024, 16, 42100−42108

(50) Sanders, V. E.; Asay, B. W.; Foley, T. J.; Tappan, B. C.; Pacheco, A. N.; Son, S. F. Reaction Propagation of Four Nanoscale Energetic Composites (Al/MoO3, Al/WO3, Al/CuO, and B12O3). *J. Propuls. Power* **2007**, *23* (4), 707−714.
(51) Son, S. F.; Asay, B. W.; Foley, T. J.; Yetter, R. A.; Wu, M. H.; Risha, G. A. Combustion of Nanoscale Al/MoO3 Thermite in Microchannels. *J. Propuls. Power* **2007**, *23* (4), 715−721.
(52) Sullivan, K. T.; Kuntz, J. D.; Gash, A. E. Electrophoretic Deposition and Mechanistic Studies of Nano-Al/CuO Thermites. *J. Appl. Phys.* **2012**, *112* (2), 024316.
(53) Du, Y.; Jin, Z.; Huang, B.; Gong, W.; Xu, H.; Yuan, Z.; Schuster, J. C.; Weitzer, F.; Krendelsberger, N. A Thermodynamic Description of the Al-Mn-Si System over the Entire Composition and Temperature Ranges. *Metall. Mater. Trans. A* **2004**, *35* (5), 1613−1628.
(54) Tu, C.; Chen, X.; Li, Y.; Zhang, B.; Zhou, C. Experimental Study of Al Agglomeration on Solid Propellant Burning Surface and Condensed Combustion Products. *Def. Technol.* **2023**, *26*, 111−122.
(55) Babuk, V. A.; Vassiliev, V. A.; Sviridov, V. V. Propellant Formulation Factors and Metal Agglomeration in Combustion of Aluminized Solid Rocket Propellant. *Combust. Sci. Technol.* **2001**, *163* (1), 261−289.
(56) Hinds, W. C. *Aerosol Technology: Properties, Behavior, and Measurement of Airborne Particles*; Wiley, 1999.
(57) Egry, I.; Ricci, E.; Novakovic, R.; Ozawa, S. Surface Tension of Liquid Metals and Alloys — Recent Developments. *Adv. Colloid Interface Sci.* **2010**, *159* (2), 198−212.
(58) Hubbe, M. A. Theory of Detachment of Colloidal Particles from Flat Surfaces Exposed to Flow. *Colloids Surf.* **1984**, *12*, 151−178.
(59) Sharma, M. M.; Chamoun, H.; Sarma, D. S. H. S. R.; Schechter, R. S. Factors Controlling the Hydrodynamic Detachment of Particles from Surfaces. *J. Colloid Interface Sci.* **1992**, *149* (1), 121−134.
(60) Chu, Q.; Chang, X.; Chen, D. A Physiochemical Model for the Combustion of Aluminum Nano-Agglomerates in High-Speed Flows. *Combust. Flame* **2022**, *237*, 111739.
(61) Basu, S.; Nandakumar, K.; Masliyah, J. H. A Model for Detachment of a Partially Wetting Drop from a Solid Surface by Shear Flow. *J. Colloid Interface Sci.* **1997**, *190* (1), 253−257.
(62) Friedlander, S. K. *Smoke, Dust and Haze: Fundamentals of Aerosol Behavior*; Oxford University Press, 1977.
(63) Dinsdale, A. T.; Quested, P. N. The Viscosity of Aluminium and Its Alloys-A Review of Data and Models. *J. Mater. Sci.* **2004**, *39* (24), 7221−7228.
(64) Bertrand, E.; Blake, T. D.; De Coninck, J. Dynamics of Dewetting. *Colloids Surf. Physicochem. Eng. Asp.* **2010**, *369* (1−3), 141−147.

https://doi.org/10.1021/acsami.4c05801
ACS Appl. Mater. Interfaces 2024, 16, 42100−42108